Molecular Neurobiology (2019) 56:6551–6565
https://doi.org/10.1007/s12035-019-1542-1

A Novel PEGylated Block Copolymer in New Age Therapeutics for Alzheimer's Disease

Sutapa Som Chaudhury[1] · Achinta Sannigrahi[2] · Mridula Nandi[3] · Vipin K. Mishra[4] · Priyadarsi De[3] · Krishnananda Chattopadhyay[2] · Sabyashachi Mishra[4] · Jaya Sil[1] · Chitrangada Das Mukhopadhyay[1]

Received: 27 November 2018 / Accepted: 27 February 2019 / Published online: 12 March 2019

Abstract

The amyloid cascade hypothesis dealing with the senile plaques is until date thought to be one of the causative pathways leading to the pathophysiology of Alzheimer's disease (AD). Though many aggregation inhibitors of misfolded amyloid beta ($A\beta_{42}$) peptide have failed in clinical trials, there are some positive aspects of the designed therapeutic peptides for diseases involving proteinaceous aggregation. Here, we evaluated a smart design of side chain tripeptide (Leu-Val-Phe)-based polymeric inhibitor addressing the fundamental hydrophobic amino acid stretch "Lys-Leu-Val-Phe-Phe-Ala" (KLVFFA) of the $A\beta_{42}$ peptide. The in vitro analyses performed through the thioflavin T (ThT) fluorescence assay, infrared spectroscopy, isothermal calorimetry, cytotoxicity experiments, and so on evinced a promising path towards the development of new age AD therapeutics targeting the inhibition of misfolded $A\beta_{42}$ peptide fibrillization. The in silico simulations done contoured the mechanism of drug action of the present block copolymer as the competitive inhibition of aggregate-prone hydrophobic stretch of $A\beta_{42}$.

Keywords Alzheimer's disease · Amyloid beta peptide · Fibrillization · Inhibitor · Peptidomimetics · M.D. simulation

Introduction

Alzheimer's disease (AD), the most common type of dementia, results in a long-term progressive impairment of cognition, memory, and other brain functionalities [1–3]. The spending on healthcare and long-term caregiving for AD-affected individuals is one of the costliest conditions to society in the current scenario. According to a report, the total expenditures for 5.7 million AD patients in the US are estimated at 277 billion US dollars in 2018 [4]. Recent estimates also indicated that AD may rank third, just behind heart diseases and cancer as a cause of death in elder people [5]. The world Alzheimer's report has highlighted that an upcoming huge drainage of the economy and deteriorated health conditions with the 131.5 million individuals worldwide are going to be affected by AD and other dementia by 2050 [6]. The pathogenesis of AD has been explained by several hypotheses, such as the amyloid hypothesis, tau hypothesis, and the latest mitochondrial cascade hypothesis [7–9]. The amyloid hypothesis suggests the fibrillization and deposition of the misfolded amyloid peptide ($A\beta_{42}$) leading to degeneration of neurons and ultimate atrophy of the brain [7, 10]. This amyloid hypothesis has nowadays been criticized with the beneficiary effects of the deposited fibrils over the more toxic and destructive oligomers of misfolded amyloid peptides. It has been postulated that the deposited fibrils may act as a sink to capture the toxic, soluble oligomers [11, 12]. In spite of this criticism, fibrillization of the misfolded $A\beta_{42}$ peptide and the production of toxic oligomers are until now considered to be one of the major hallmarks of AD pathogenesis [13–16]. The credibility of the amyloid hypothesis has once again

Electronic supplementary material The online version of this article (https://doi.org/10.1007/s12035-019-1542-1) contains supplementary material, which is available to authorized users.

✉ Chitrangada Das Mukhopadhyay
chitrangadam@chest.iiests.ac.in

[1] Centre for Healthcare Science and Technology, IIEST, Shibpur, P.O. Botanic Garden, Howrah, West Bengal 711103, India

[2] Structural Biology & Bioinformatics Division, CSIR-IICB, Kolkata, 4, S.C. Mallick Road, Jadavpur, Kolkata, West Bengal 700032, India

[3] Department of Chemical Sciences, IISER Kolkata, Mohanpur, Nadia, West Bengal 741246, India

[4] Department of Chemistry, IIT Kharagpur, Kharagpur, West Bengal 721302, India

been strengthened based on the recent success of anti-amyloid antibody "Aducanumab" which has already entered the phase III trial [17]. Hence, the pathway starting from Aβ_{42} monomer oligomerization and leading to the deposition of amyloid plaques is an undeniable target in the field of drug development against AD [18–21]. Molecular chaperones, namely brichos, Hsp 70, and Hsp 90, have been proven to inhibit Aβ_{42} peptide fibrillization [22, 23]. A novel small molecule, D737, showed its efficiency as an inhibitor of misfolded amyloid beta peptide oligomerization as well as fibril formation [24]. Epigallocatechin-3-gallate and other polyphenols from natural resources were proved to significantly modulate amyloid precursor protein (APP) cleavage and thereby reduce cerebral amyloidosis [25]. Peptide-based β-sheet breakers are being tested since 1998 through the report of a pentapeptide by Soto and his colleagues [26]. Until date, many supramolecules, compounds from natural resources and peptide-based inhibitors, are in the pipeline for procuring remediable drug against AD, but none of them has been reported to pass the final clinical phase trials [27–33]. Actually, the reason why the amyloid reduction therapies do not get full success in clinical trials are that long before the onset of AD, neurodegeneration starts and scientists lacking any detectable biomarker miss that "therapeutic window" to treat AD [34]. In this milieu, the peptidomimetics have drawn a great attention from the researchers being comparatively safer drug candidates targeting Aβ_{42} fibrillization inhibition [26, 29, 35]. While some unnatural, modified amino acids have been studied for the better stability and passage through the blood–brain barrier (BBB), the natural amino acids in peptidic inhibitors are better aspirants of drug composition from the perspective of biodegradation [35, 36]. Here, we report an assessment of the simplest, PEGylated block copolymer with two varying molecular weights having leucine-valine-phenylalanine (LVF) tripeptide side chains for the inhibitory action against Aβ_{42} fibrillization. The amphiphilic PEG group is attached to the backbone of the polymer via the chain transfer reagent 4-cyano-4-(dodecylsulfanylthio-carbonyl) sulfanylpentanoic acid (CDP) to prevent the proteolytic degradation of biopolymer in the in vivo system and also to increase bioavailability of the compound as a successful drug candidate. PEGylation also makes the compound resistant to non-specific protein interaction and cellular interferences and thereby increases its stability and pharmacokinetic properties for becoming a better water-soluble drug candidate [37]. With the natural L-form of amino acids leucine, valine, and phenylalanine, the inhibitory compound has been proven with its minimal or no side effect on cultured neuroblastoma cells viz. SHSY5Y as expected. In some previous reports, PEG-poly-lactic acid nanoparticles and liposomes were shown as promising nano drug-carrier loaded with β-sheet breaker peptides for neurodegenerative diseases like AD [38, 39]. Heading towards future AD therapeutics, the present block copolymers of ours may be modified as a drug vehicle loaded with any symptomatic drug like memantine or donepezil to provide a combinatorial theragnostic tool.

Materials and Methods

Synthesis and Characterization of the PEGylated Tripeptidic Block Copolymers

The PEGylated tripeptidic block copolymers having two different molecular weights [(PEG_{2K}-*b*-P (LVF-HEMA)$_{6K}$ (Inhibitor 1, I1) and (PEG_{5K}-*b*-P (LVF-HEMA)$_{6K}$ (Inhibitor 2, I2)] were synthesized following the protocol reported previously by Kumar et al. with a twist in the attachment site of PEG [40]. The monomer Boc-Leu-Val-Phe-oxyethyl methacrylate (Boc-LVF-HEMA) was synthesized following standard procedure [40]. These monomeric blocks were, then, homopolymerized via reversible addition-fragmentation chain transfer (RAFT) polymerization reaction. To procure this, Boc-LVF-HEMA (500 mg, 0.85 mmol), chain transfer agent (CTA), $mPEG_{2K}$-4-cyano-4-(dodecylsulfanylthiocarbonyl) sulfanylpentanoic acid ($mPEG_{2K}$-CDP) (101 mg, 0.04 mmol), 2,2-azobisisobutyronitrile (AIBN) (0.7 mg, 4.24 μmol), and anhydrous N,N-dimethylformamide (DMF) (1.25 g) were placed in a septa-sealed vial aided with a magnetic stir bar. The vial was purged with dry N_2 for 20 min before placing in the pre-heated reaction block at 70 °C. The polymerization was stopped by cooling the vial in an ice-water bath and exposing the reaction mixture to air. After quenching, the reaction mixture was diluted with acetone and precipitated from hexanes. The block copolymer, (PEG_{2K}-*b*-P (LVF-HEMA)$_{6K}$, was further re-precipitated around five times from acetone/hexanes and dried under high vacuum for 8 h at 35 °C to obtain faint yellowish polymers. Monomer conversion was determined gravimetrically from the initial weight of monomer taken and that of the purified polymer. A similar procedure was followed for the synthesis of (PEG_{5K}-*b*-P (LVF-HEMA)$_{6K}$ block copolymer. This resulting Boc-protected polymer P (Boc-LVF-EMA) was, then, converted into Boc-de-protected polymer salt P (CF_3COO-H_3N^+-LVF-HEMA) by taking 160.0 mg P (Boc-LVF-HEMA) in 2.0 ml DCM with 0.5 ml trifluoroacetic acid (TFA) added drop-wise at ice-water bath under the stirring condition at RT for 2 h. The deprotected polymer was precipitated in cold diethyl ether and dried under vacuum for 8 h at 35 °C (Scheme 1 and Table S1). Boc group deprotection was confirmed by ^{1}H NMR spectroscopy. Size and morphology of these polymers were

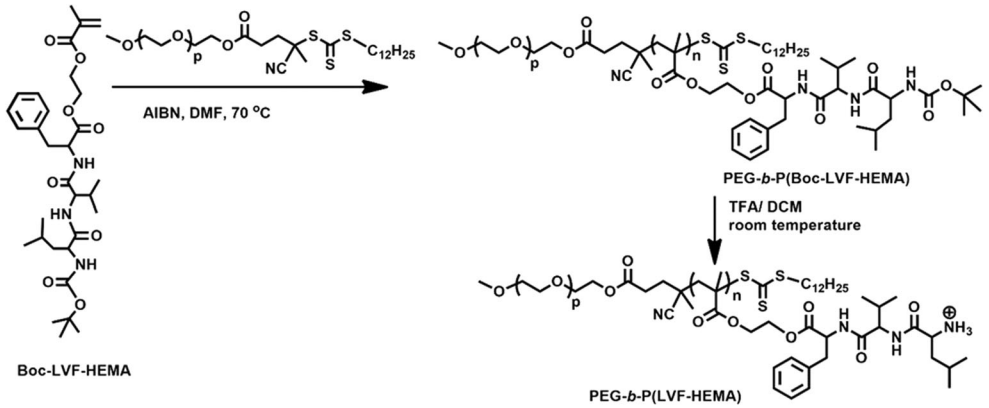

Scheme 1 Synthesis of amphiphilic PEGylated block copolymer PEG-*b*-P (LVF-HEMA) via reversible addition-fragmentation chain transfer (RAFT) polymerization in DMF at 70 °C, followed by Boc group deprotection at room temperature

characterized with the aid of field emission scanning electron microscopy (FE-SEM) and dynamic light scattering (DLS) profiling and their secondary structures were determined via the CD spectra. The cytotoxicity of the inhibitors was assessed on the neuroblastoma cell line SHSY5Y as well as breast cancer cell line MCF-7.

Amyloid Beta Preparation

Following a modified protocol of Reinke et al., 1 mg sample of the synthetic Aβ_{42} peptide (Sigma Aldrich) was dissolved in 200 μL 1,1,1,3,3,3-hexafluoroisopropanol (HFIP) [41]. HFIP was, then, removed with the aid of a SpeedVac, and the obtained thin film was stored at − 20 °C until use. Before every single experiment, a 0.1 mg aliquot from this stored Aβ_{42} was re-suspended in DMSO followed by 20 mM phosphate buffer saline (PBS) pH 7.4, to a final concentration of 100 μM (10% final DMSO concentration). Aliquots were, then, sonicated for 1 min at RT and, thus, ready to use.

Amyloid Beta Oligomer Preparation

Aβ_{42} oligomer was prepared following the protocol of Saleem and Biswas [42]. Lyophilized Aβ_{42} was equilibrated at RT for 30 min and suspended in HFIP to a concentration of 1 mM. Then, HFIP was allowed to evaporate in a SpeedVac for about 45 min. This aliquot was re-suspended in anhydrous dimethyl sulfoxide (DMSO) to a concentration of 5 mM by pipette mixing followed by bath sonication for 10 min and stored at − 80 °C until use. Prior to the experiment, this 5 mM stock was diluted with PBS to a concentration of 400 μM and incubated at 37 °C for 24 h following addition of 0.2% sodium dodecyl sulfate (SDS). After 24 h, this was again diluted with 1× PBS to a final concentration of 100 μM and incubated at 37 °C for another 24 h.

Thioflavin T Fluorescence Assay

Aβ_{42} was dissolved in 20 mM PBS (pH 7.4) at a concentration of 15 μM (based on the toxic dose tested in vitro, Fig. 6). Interaction of the polymeric inhibitors (8 and 11 K) with the Aβ_{42} was tested in 1:1 to 1:3 molar ratio at a fixed concentration of 15 μM Aβ_{42} for 5 days of incubation at 37 °C in shaking condition at 180 rpm. In one treatment set, the inhibitors were added to the Aβ_{42} from the beginning of incubation, and, in another set of treatment, they were added at a later stage (after 24 h) of Aβ_{42} incubation. This was done to evaluate whether the inhibitors were able to inhibit fibril formation as well as had a capability to degrade the preformed fibrils. The inhibition of fibrillization and pre-formed fibril degradation was measured using thioflavin T (ThT) fluorescence assay following a modified protocol of Kyung Hyun Lee et al. [43]. Briefly, 1 μl, 5 mM ThT in 20 mM PBS (pH 7.4) was added to 25 μl of 15 μM Aβ_{42} (and/or 1:1, 1:2, and 1:3 treatment of Aβ_{42}:inhibitor) in 475 μl 20 mM PBS (pH 7.4). The excitation and emission wavelengths were 450 and 485 nm, respectively, with a bandwidth of 5 nm. The measurements were recorded using an integration time of 0.2 s in a Photon Technology International (PTI) fluorimeter. To check the effectiveness of the inhibitors against Aβ_{42} oligomer, 3 sets of treatment with the Aβ_{42} oligomer and 2 inhibitors in 1:1 to 1:3 molar ratios of oligomer and inhibitors were incubated in a similar way as stated previously. Aβ_{42} oligomer was taken at a fixed concentration of 12 μM (the toxic dose tested in vitro, Fig. 6) for each case. ThT assays for these oligomers were performed in a similar manner with that of the fibrils.

The ThT fluorescence spectra of I1 and I2 were considered as the control one.

Dynamic Light Scattering Analyses

Dynamic light scattering (DLS) analyses were performed to have a gross idea about the size and the morphology of the block copolymers, as well as the transformation of the Aβ_{42} fibrils and oligomers on interaction with the inhibitors. The data were obtained measuring the scattered light at a scattering angle θ of 173° at RT, using a 4 mW He–Ne laser of wavelength 632.8 nm. At the time of measurement of the diameter of two inhibitors, the block copolymers were dissolved in deionized water at a concentration of 15 μM and the reaction mixtures of Aβ_{42} fibrils/oligomers and the inhibitors of different concentrations were set in a PBS solution of 20 mM, pH 7.4. DLS analyses were carried on a Zetasizer Nano ZS, Malvern Instrument, UK.

Atomic Force Microscopy

Aliquots of control Aβ_{42} fibril, oligomer, and the inhibitor-treated fibrils and/or oligomers at a concentration of 1 μM (in treatment fibril/oligomer and I1 & I2 were taken in 1:1 ratio, respectively) were drop-casted on clean, acetone-washed glass coverslips. These coverslips were kept in boxes with their mouth covered with tissue paper to air dry the solution for 2–3 days and, then, placed in a vacuum desiccator for 1 h and were imaged using a semi-contact mode at a scan rate of 1 Hz of the instrument. Commercial NSG tips from NT-MDT were used as atomic force microscopy (AFM) probes, and 1 V voltage was applied to the tip for AFM scan. AFM micrographs were captured under an NT-MDT micro-40 AFM instrument.

Field Emission Scanning Electron Microscopy

The 1 μM solution of inhibitors, the treated fibril, and the oligomer samples were drop-casted as stated previously in the AFM section. The gold:palladium (20:80)-coated samples were imaged under high-performance variable pressure field emission scanning electron microscopy (FE-SEM) with patented GEMINI column technology using Schottky-type field-emitter system, single condenser with crossover-free beam path. FE-SEM images were taken from SUPRA 55VP-Field Emission Scanning Electron (Zeiss) microscope.

Transmission Electron Microscopy

Control Aβ_{42} fibril, oligomer (not incubated as the other samples), and the inhibitor-treated fibrils and/or oligomers at a concentration of 1 μM in 1:1 ratio, respectively, were placed on carbon-coated copper grids. After removing the excess sample with tissue, the grids were air-dried and observed under a JEM-2100 plus electron microscope (JEOL, Tokyo, Japan).

Circular Dichroism Spectroscopy

Conformational changes of Aβ_{42} fibril upon binding to the inhibitors were evaluated with the aid of far-UV circular dichroism (CD) spectroscopic studies, using a JASCO J720 spectropolarimeter, Japan Spectroscopic Limited. Far-UV CD measurements (between 190 and 250 nm) were performed using a cuvette of 1 mm path length and keeping the scan speed at 50 nm/min with response time at 2 s. Bandwidth was set at 1 nm, and the final spectra were recorded as an average value of three CD spectra recorded in continuous mode. The protein concentration of 45 μM (control Aβ_{42} fibril and oligomer and 1:1 fibril/oligomer and inhibitor) was used for the CD measurements.

Fourier Transform Infrared Spectroscopic Studies

Liquid-state Fourier transform infrared (FT-IR) analyses were performed in support of the CD spectral analyses. Aβ_{42} fibril and the inhibitor-treated fibrils were taken at a concentration of 1 μM each in 20 mM PBS buffer, pH 7.4. The buffer baseline was subtracted each time prior to the recording of spectral readout. The raw spectra were de-convoluted in β-sheet to turn region (1610–1795 cm^{-1}) by least-square iterative curve fitting to Gaussian/Lorentzian line shapes. The analyses of the percentage of β-sheets and α-helix population were determined using the previously reported data by Ahmed et al. [44]. FT-IR spectra were recorded using a Bruker 600 series FT-IR spectrometer.

Cell Viability Assay

The stored Aβ_{42} and preformed Aβ_{42} oligomers were dissolved in 20 mM PBS (pH 7.4) at a concentration range of 10–500 μM and incubated for 72 h at 37 °C in shaking condition at 180 rpm, in the presence or absence of I1 and I2, at a molar ratio of 1:1, 1:2, and 1:3. At the time of the experiment, these were diluted 10 times with the high-glucose Dulbecco's modified Eagle's media (DMEM). Control experiments were performed on the cells growing on the medium alone and on the inhibitors alone at the same working concentration used for the fibrillization/oligomerization inhibition tests. For testing the cytotoxicity of the inhibitor compounds, the cell viability was tested over the range of 1–100 μM working concentrations on SHSY5Y neuroblastoma cell line as well as on breast cancer cell line MCF-7.

SHSY5Y and MCF-7 cells were maintained in high-glucose DMEM supplemented with 10% fetal bovine serum (FBS) and 500 μg/ml solution of penicillin/streptomycin.

Following a standard procedure, the viability assays were performed [45]. Briefly, cells were seeded in 96-well plates at a density of 10,000 cells per well in 100 μl high-glucose complete DMEM and allowed to grow for 24 h under 5% CO_2 at 37 °C. After 24 h, the medium was replaced with that containing the pre-incubated treatment as stated previously. Again, after 24 h incubation in the same condition, 10 μl MTT reagent (5 mg/ml in PBS) was added in each well and allowed to incubate for 4 h at 5% CO_2 at 37 °C. Then, 85 μl medium was removed from each well, and the resulting insoluble formazan was dissolved in 50 μl DMSO. This was allowed to stand for 10 min at the CO_2 incubator at 37 °C, and the absorbance was measured with the aid of a spectrophotometric microplate reader at 570 nm wavelength. The medium without cells was taken as a blank and subtracted as background from each sample. Absorbance spectra in 3-(4,5-dimethylthiazol-2-yl)-2,5-diphenyltetrazolium bromide (MTT) reduction assays were recorded using a BioRad iMark™ microplate reader.

Ligand Binding and Molecular Dynamics Simulation

Atomistic molecular dynamics (MD) simulations were carried out to describe the interaction of the ligand (PEGylated inhibitor) with the fibril and oligomer of Aβ_{42}, as well as with the Aβ_{42} monomeric peptide and the hydrophobic stretch–KLVFFA segment of the monomeric Aβ_{42} peptide. The initial structures of fibril, oligomer, monomer, and KLVFFA segment of the monomer were taken from the crystal structures corresponding to the PDB id 5KK3, 4q8d, 1IYT, and 2Y2A, respectively [46–49]. The polymeric ligand used in the experiment was modeled in its truncated form (Fig. 7b). The systems were solvated in orthorhombic water box with dimensions of 115 Å × 110 Å × 90 Å for monomers, 70 Å × 70 Å × 50 Å for oligomers, and 155 Å × 75 Å × 75 Å for the fibril system. The charges of the system were neutralized, and an ionic concentration of 0.15 M was achieved by adding Na^+ and Cl^- ions. The systems were, then, slowly heated to 300 K and equilibrated for 5 ns constant temperature and volume (NVT ensemble), followed by a 50 ns molecular dynamics run at constant temperature (300 K) and constant pressure (1 atm) using the Nose-Hoover Langevin thermostat and piston (NPT ensemble). All simulations were done with the only hydrogen containing bonds constrained by SHAKE. An integration time step of 2 fs was used, and structures were saved every 5 ps for analysis. The long-range electrostatic interactions were treated by the particle mesh Ewald (PME) method with a 12 Å cutoff. The van der Waals interactions were truncated at a cutoff of 12 Å, and a switch function was activated starting at 10 Å. All simulations were performed employing the NAMD program with the CHARMM22 force field and TIP3 potential for water molecules, and Charmm general force field for ligand was generated from the Paramchem suite [50–53]. The analysis and visualization were done using VMD and PYMOL software [54, 55].

In the computer-based MD simulation study, the fragmentation of fibril bound to the inhibitors was examined in terms of root mean square deviation (RMSD) and secondary structure analysis, in addition to the binding energetics (electrostatic and Van der Waals energy) study between ligand and fibril.

Kinetics Study: Isothermal Titration Calorimetry

The changes in enthalpy upon binding of Aβ_{42} monomer/fibril with the inhibitors were measured using a high-sensitivity isothermal titration calorimeter (ITC), a MicroCal iTC_{200}, UK instrument and following the method reported elsewhere [56]. A total of 350 μl of 8 μM protein samples (Aβ_{42} monomer/fibril) and 40 μl of 5 mM I1 and I2 were filled at the sample and reference cells, respectively, of a calorimetric cell. A series of 20 injections with 2 μl each of protein sample at 240 s time interval were performed in the ITC cell, and the characteristic heat signal from absorbed or released heat by the interaction of protein-inhibitor per injection generated the endothermic and exothermic signals. The heat of dilution was calculated by injecting the buffer at sample cell. The ITC thermogram was obtained by integrating the heat signals and subtracting the heat of dilution and finally fitted to a sequential binding model by Microcal origin to have the binding constant (K) and molar enthalpy of interaction (ΔH). The Gibb's free energy was calculated from $\Delta G = -RT \ln(55.5\ K)$, and the entropic contribution was estimated following the equation $\Delta G = \Delta H - T\Delta S$, where the water concentration (55.5 M) was used to correct the unit of K to the molar fraction.

Statistical Analyses

The experimental data were expressed by calculating the standard error of the mean from 3 individual experimental data, and the levels of significance were analyzed by Student's *t* test, where $P < 0.05$ was considered as statistically significant.

Results

Characterization of the PEGylated Block Copolymers

Boc group deprotection and the purity of the side chain tripeptide-based polymeric inhibitors were confirmed by ^1H NMR spectroscopy (Fig. S1). Both the polymers were soluble in water. The polymeric inhibitors have an average size of around 30 nm in diameter, as shown in the DLS and FE-SEM analyses (Figs. S2, S3). The CD profiles (Fig. S4) recorded at physiological pH of 7.4 revealed the β-sheet nature of the inhibitors.

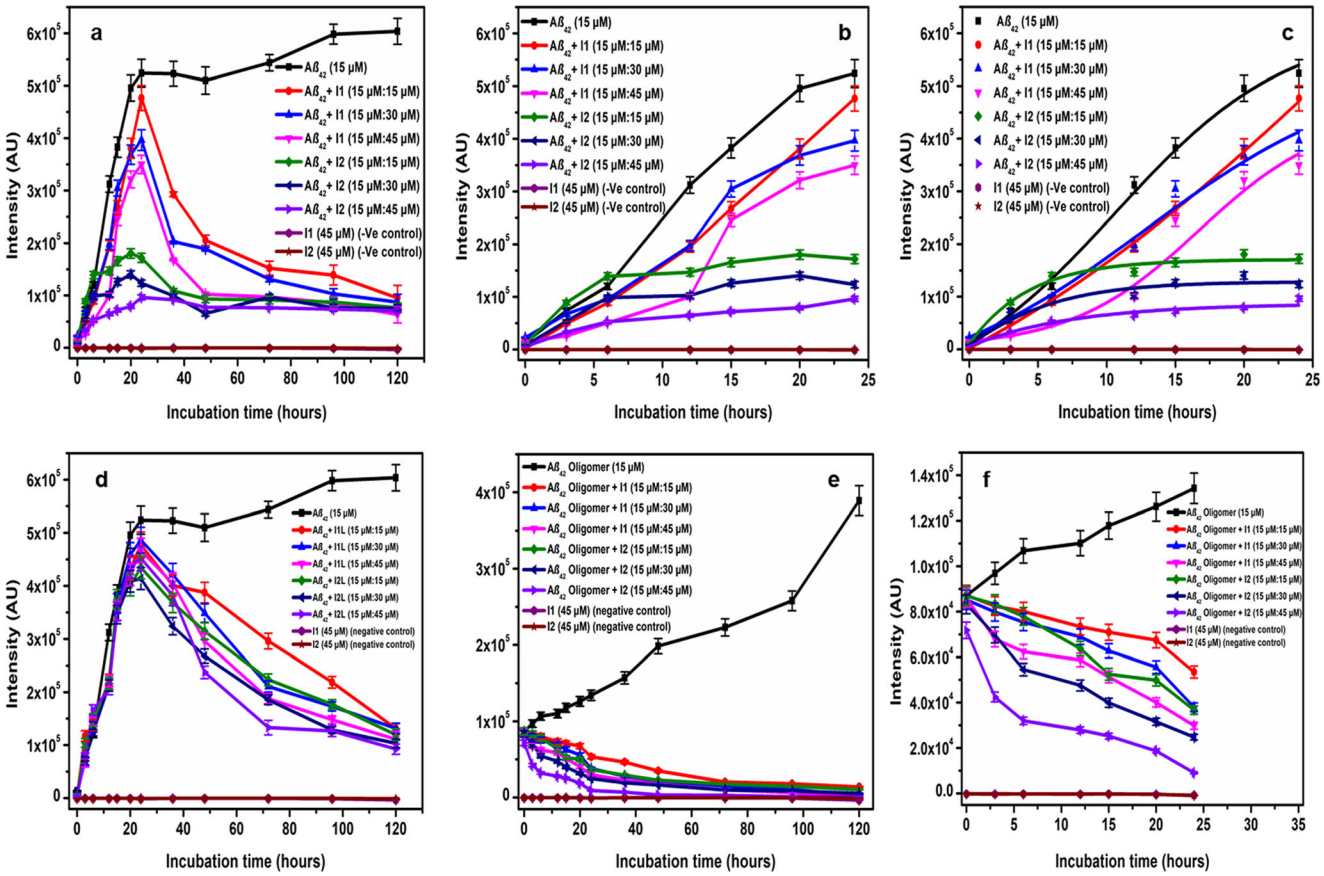

Fig. 1 Quantitative measurement of Aβ_{42} fibrillization inhibition by ThT fluorescence assay. **a** Fibril degradation by I1 and I2; **b** a closer look to fibril formation of Aβ_{42} peptide and respective inhibitory action of the inhibitors until 24 h; **c** fitted curve of (**b**) indicating significant reduction in the aggregation rate in the presence of I1 and I2 with increasing concentration; **d** degradation of preformed fibril on addition of I1 and I2 after 24 h of incubation (I1L and I2L indicate the inhibitors added at a later stage of incubation, i.e., 24 h); **e** targeted destruction of Aβ_{42} oligomers; **f** a closer look at oligomer to fibril formation in the absence and presence of I1 and I2. Error bars indicate the standard error of mean from 3 experimental data

The Early-Stage Inhibitory Effect of Block Copolymers on Aβ_{42} Fibrillization

The emitted ThT fluorescence intensity at 485 nm wavelength reflected that I2 spontaneously inhibited the formation of toxic oligomers from the major monomeric fraction of the synthetic Aβ_{42} solution [57, 58]. Whereas, I1 though present in the solution since the zeroth hour of incubation showed its efficiency in degrading the pre-formed fibrils after 24 h (Fig. 1a, d). Eventually, when inhibitors were added at a later stage of incubation (after 24 h), both of them helped in degradation of the predestined fibrils (Fig. 1d). The inhibitors exhibited an increasing effectivity when tested with increasing molar ratios of 1:1 to 1:3 with respect to the fixed concentration of Aβ_{42} peptide, i.e., 15 μM. To detect the fate of Aβ_{42} oligomers on treatment with 1:1 to 1:3 equimolar I1 and I2, the changes in fluorescence intensity were continuously monitored. A steady decrease in emitted fluorescence intensity over an incubation period of 5 days clearly signified the successful binding and subsequent degradation of Aβ_{42} oligomers at the concentration of oligomers, i.e., 12 μM tested with 1:1 to 1:3 M ratio of the inhibitors, respectively. I1 and I2 at a concentration of 45 μM showed no significant increase in the fluorescence intensity and thus were taken as negative controls. In all cases, I2 showed a more promising result in comparison to I1. The higher amount of PEG group in I2 as compared to I1 (PEG_{5K} versus PEG_{2K}) might be responsible for making I2 more water soluble and a better performer as an inhibitor [59].

The decrease in the size of Aβ_{42} fibrils as evidenced in the DLS measurements also supported the results obtained from the ThT fluorescence assay. Aβ_{42} alone upon incubation over 5 days showed fibrils with an average size of 1000 nm. When Aβ_{42} treated with I1 and I2 respectively at 1:1 ratio formed a mixture of oligomeric/monomeric entities much below the size of 1000 nm (Fig. S6) which did not revert back into fibrillar stage again over five days of treatment. Here, also, the better performance of I2 was reflected.

Inhibition of Aβ_{42} fibrillization, fibril degradation and degeneration of oligomers were directly documented with the AFM, FE-SEM, and transmission electron microscopy (TEM) images. The Aβ_{42} fibrils were prominent when incubated in absence of any of the inhibitors. However, long fibrils were

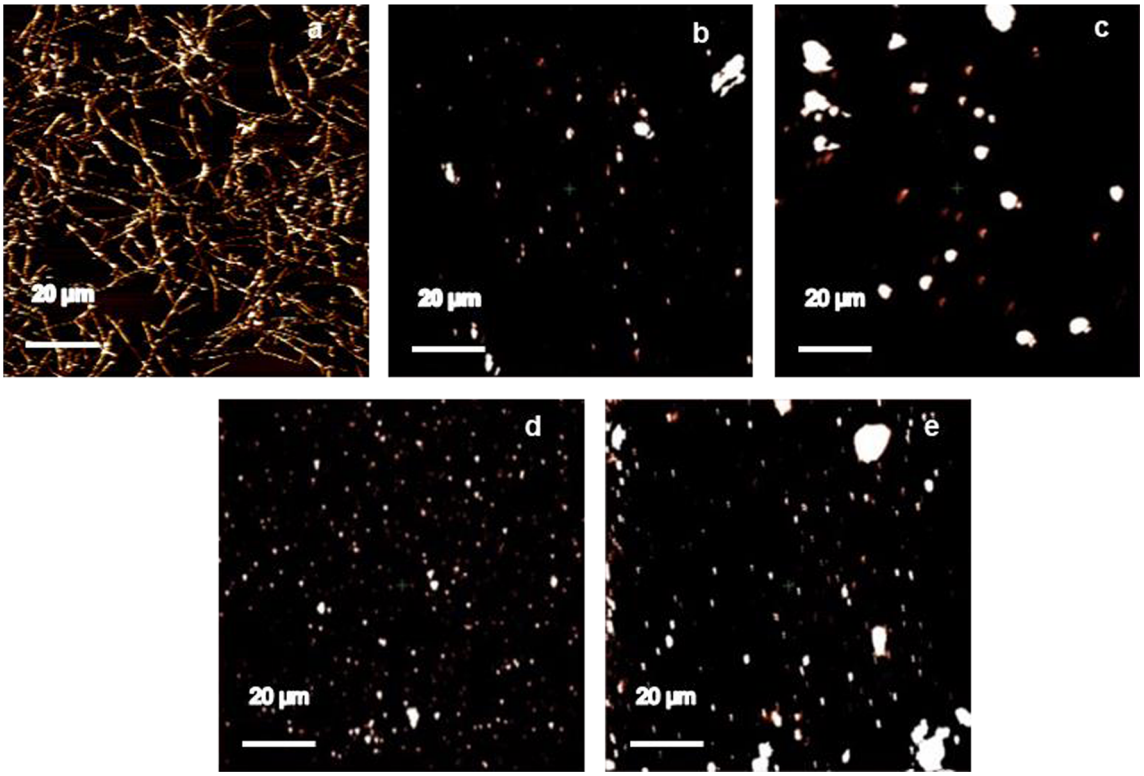

Fig. 2 AFM images showing effect of the inhibitors. **a** Aβ_{42} fibrils in the absence of any inhibitor; **b** degraded fibrils (1 μM) incubated with 1 μM I1 from initial point; **c** for I1 added at a later stage, i.e., 24 h; **d** for I2 present from the initiation of incubation; **e** for I2 added at a later stage, i.e., 24 h. The scale bar corresponds to 20 μm

not observed in the presence of the inhibitors (Figs. 2–4). When the Aβ_{42} oligomers were treated with the equimolar concentration of the inhibitors, the degraded oligomers were found along with the presence of clustered inhibitors as observed in the FE-SEM images (Fig. 3e, f). Moreover, it was found that in presence of the inhibitors the oligomers were not able to reassemble themselves into long fibrils again (Fig. 4d–f).

Aβ_{42} peptide on incubation at 37 °C for 3 days showed a switching from a naïve α-helix to a β-sheet rich conformation. This switching of the α-helical secondary structure of Aβ_{42} monomeric population into β-sheet rich conformation was reflected by the delta ellipticity maximum at 216 nm in far-UV CD spectra. When the Aβ_{42} peptide was incubated along with the inhibitors, a complete disruption of β-sheet conformation was observed considering the CD spectral shift at 208 and 222 nm wavelength (Fig. 5). Moreover, the characteristic positive peak at around 196 nm wavelength which indicates the turns in β-sheet was found to be decreased in the treated Aβ_{42} samples as compared to the control fibril (red line). Also, this decreased peak at 196 nm reflected a resemblance with that of the Aβ_{42} peptide at "0" h. Thus, the conformational change of Aβ_{42} peptide was evaluated with the aid of CD spectral change.

FTIR spectral readings of the Aβ_{42} peptide in the absence and presence of I1 and I2 manifested a characteristic pattern change. This was obtained by the Gaussian/Lorentzian curve fitting of raw data after deconvolution into β-sheet to turn region (Fig. S7). Prior to incubation at 37 °C, the freshly prepared phosphate buffer saline (PBS) solution of Aβ_{42} displayed an absorbance maximum of 1642 cm^{-1} with two shoulders at 1600 cm^{-1} and 1680 cm^{-1} in the amide I region, corresponding to the α-helix conformation [60, 61]. Following the incubation, a conformational shift from α-helix to β-sheet occurred which was evidenced by the shift in absorbance maximum. The incubated control fibril showed maximum absorbance peak at 1610 cm^{-1} with one band at 1650 cm^{-1}, which is the characteristic profile of β-sheet conformation [62–64]. Moreover, the treated fibril with I1 and I2 exhibited a spectral shift away from the β-sheet region. In both these cases, we found the absorbance maximum at 1600 cm^{-1} with one band at 1675 cm^{-1} (Fig. S7 and Table S2). Analysis of the fitted curves revealed the percent occurrence of different conformations. Aβ_{42} peptide at the initial stage of incubation contained 21.47% β-sheet and 42.71% α-helix which upon aggregation gave rise to 52.37% β-sheet. Again, I1 and I2 on reacting with the fibril decreased the β-sheet conformation of the fibril to 19.38% and 19.73% respectively.

Cytotoxicity Assays

To evaluate the potentiation of the inhibitors as drug candidates, a series of cell viability tests were done on the neuroblastoma cell line, SHSY5Y. From the cytotoxicity assay, I1 and I2 were found

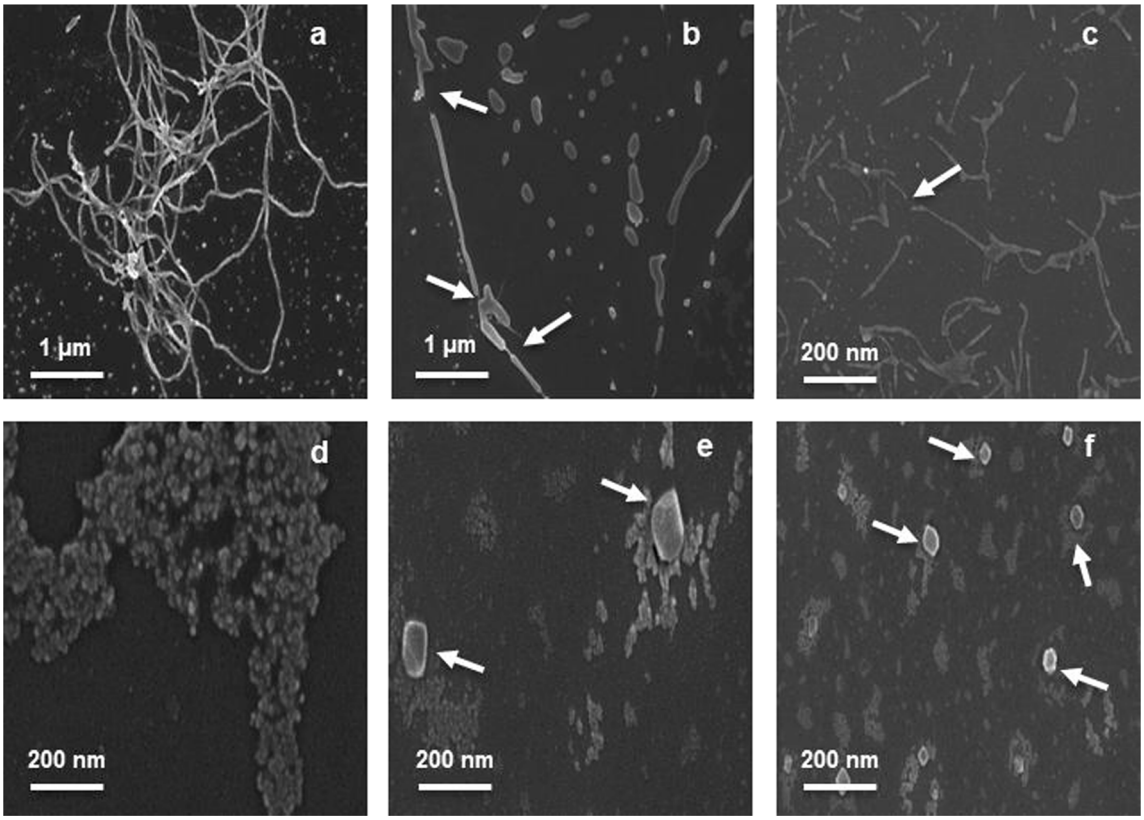

Fig. 3 Field emission scanning electron micrographs of control Aβ_{42} fibril and oligomer and their respective treatments; **a** control fibril, **b** fibril + I1, **c** fibril + I2, **d** control oligomer, **e** oligomer + I1, **f** oligomer + I2. The fibril-cleavage sites are indicated with the white arrows. The clusters of the inhibitors were visible along with degraded oligomers in (**e**) and (**f**) (marked with the white arrows)

to be nontoxic up to a high concentration of 45 and 55 μM, respectively (Fig. S5a). Although, on testing the cytotoxicity of I1 and I2 on breast cancer cell line, MCF-7, within the range up to 65 μM the IC-50 value could not be determined and the drugs showed no cytotoxicity within this range (Fig. S5b).

When cells were treated with Aβ_{42} preformed fibril in the absence of inhibitors, the cell population was reduced to 38% at a concentration of 15 μM Aβ_{42}, whereas, the fibril-I1 complex successfully raised a cytoprotective effect and increased the cell viability to 64% in comparison to the control one. The Aβ_{42} fibril-I2 complex also increased the cell viability to 54% from 38% at an equimolar concentration of 15 μM Aβ fibril and I2 (Fig. 6). The treatment of oligomers in the presence of I1 and I2 resulted in an increased cell population to 18 and 36%, respectively, in comparison to the 10% viability of the control oligomer at 12 μM concentration (Fig. 6). Significant changes in the cell survival were also observed in the case of the fibril and/or oligomers and the inhibitors incubated in 1:1, 1:2, and 1:3 ratios (Fig. 6).

In Silico Molecular Dynamics Studies

To understand the mechanism of drug action, in silico molecular dynamics (MD) simulations were carried out [65, 66]. Based on the design of inhibitors, we hypothesized that leucine, valine, and phenylalanine moieties of PEGylated polymers may act as competitive inhibitors of the 17-Leu-Val-Phe-19 stretch of pathogenic Aβ_{42}. The simulations were run to validate this hypothesis and to register any conformational change of Aβ_{42} peptide upon binding of the ligand (inhibitor).

Interaction of ligand with KLVFFA segment of monomeric Aβ_{42} In several previous studies, the KLVFFA segment of the monomeric Aβ_{42} peptide has been demonstrated as the self-assembling hydrophobic stretch leading to the formation of cytotoxic oligomers and the fibrillar deposits [67]. To test the competitive inhibitory action of the ligand, the interaction of the self-assembling KLVFFA segment and the ligand was followed. The 50 ns MD simulation of six units of KLVFFA segment of Aβ_{42} (in the absence of ligand) presented a general tendency of the individual segments to come close to each other during the course of the simulation (Fig. S8). Though, the aggregated units being highly dynamic in nature were short-lived during that time span. On simulating six units of KLVFFA segment together with the ligand, a strong interaction persisted between one or two KLVFFA segment and the hydrophobic side chains of the ligand. This led to the stoppage of further aggregation of KLVFFA units compared to what was seen in the simulation of six KLVFFA units in the absence of the

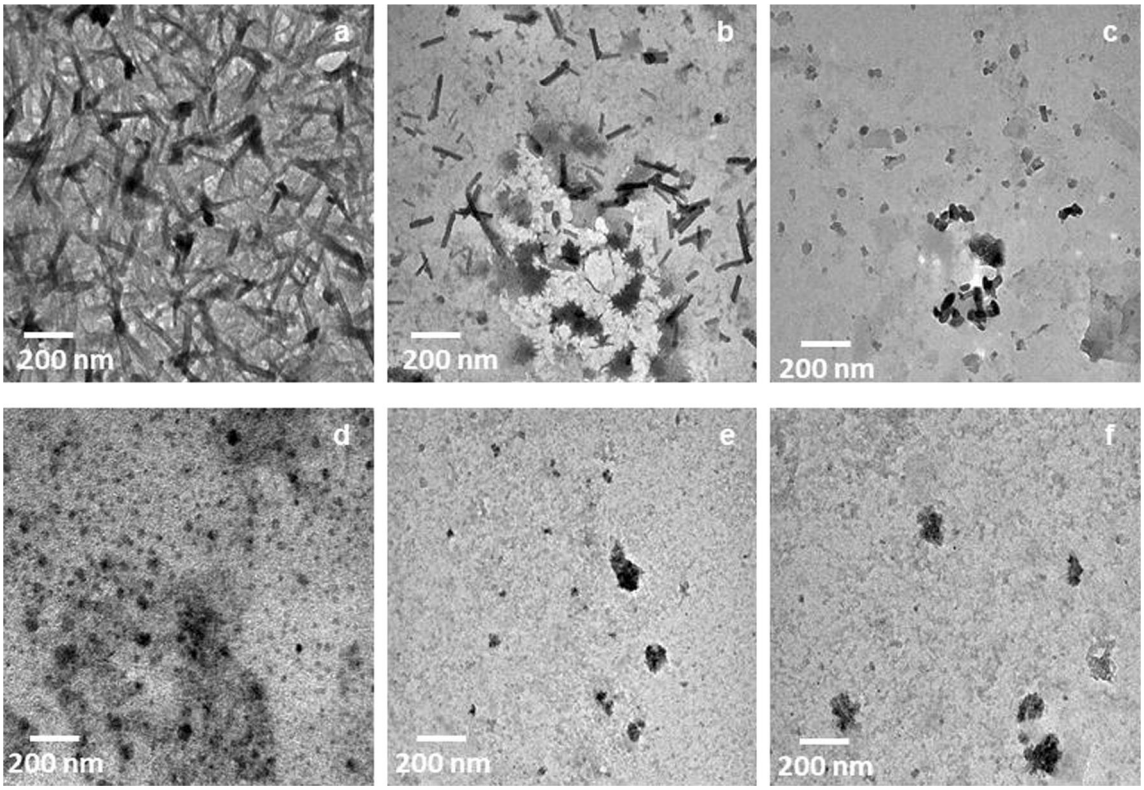

Fig. 4 TEM images of Aβ_{42} after incubation at 37 °C for 5 days in the absence and in the presence of I1 and I2; **a** Aβ_{42} fibrils at day 5, as control **b** fibril + I, **c** fibril + I2, **d** control oligomer (non-incubated), **e** oligomer + I1 at the end of day 5, and **f** oligomer + I2 on day 5. Aβ_{42}:I1 and Aβ_{42}:I2 were taken in 1:1 molar ratio. The scale bar corresponds to 200 nm

ligand (Fig. S9). A detailed secondary structure composition in the MD simulation of both of the systems (ligand-bound and unbound states of six KLVFFA units) was analyzed (Fig. S10). This delineated the aggregation of individual KLVFFA segment via the formation of the helix and isolated bridge during 80 ns MD simulation as shown in Fig. S10a [68]. However, this type of helix and isolated bridge formation was not observed in the presence of the ligand as depicted in Fig. S10b. Moreover, a notable change was seen in the increased occurrence of isolated bridge and helix in the six KLVFFA segments in the absence of the ligand. This finding suggested that the ligand interacts with KLVFFA segment of monomeric Aβ_{42} peptide strongly and diminishes the aggregation of self-assembling KLVFFA segments by inhibiting the formation of isolated bridge structures and turns.

Interaction of ligand with fibril On the basis of overall conformational dynamics of the system, the fibril was found to retain its structural rigidity in the absence of the ligand. However, when the ligand was present, the conformational dynamics of the fibril was enhanced, as seen from the RMSD fluctuation of the Cα atoms of fibril in the presence and absence of the ligand (Fig. 7a). Upon investigation of conformational dynamics of the individual chains in the fibril, it was found that the chains, which were exposed to interaction (Fig. 7c) with the ligand showed much larger RMSD fluctuation at the time of existence of ligand, whereas other chains (that were not exposed to the ligand) showed similar conformational dynamics in the presence and absence of the ligand (Fig. 7d). The larger RMSD fluctuation was indicative of the

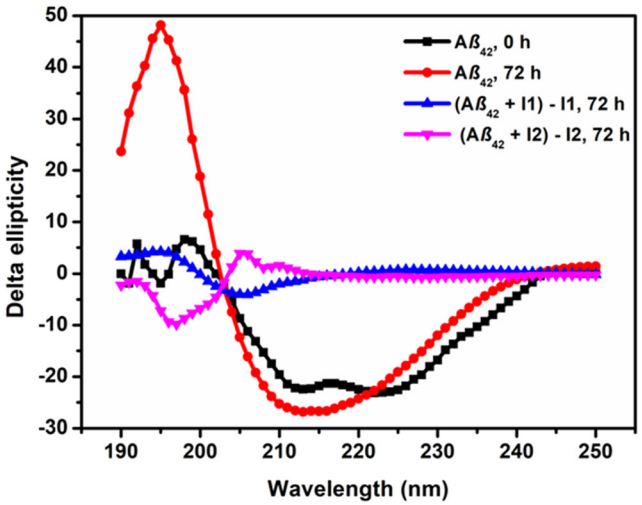

Fig. 5 Comparisons in the CD profile before and after the inhibitor treatment. The red line indicates the fibril formed after incubation, the blue line indicates the absolute change in the β-sheet after treatment with I1 (fibril + I1-I1), and the pink line indicates the absolute change in the β-sheet after treatment with I2 (fibril + I2-I2). Here, absolute quantity indicates the data obtained after normalization

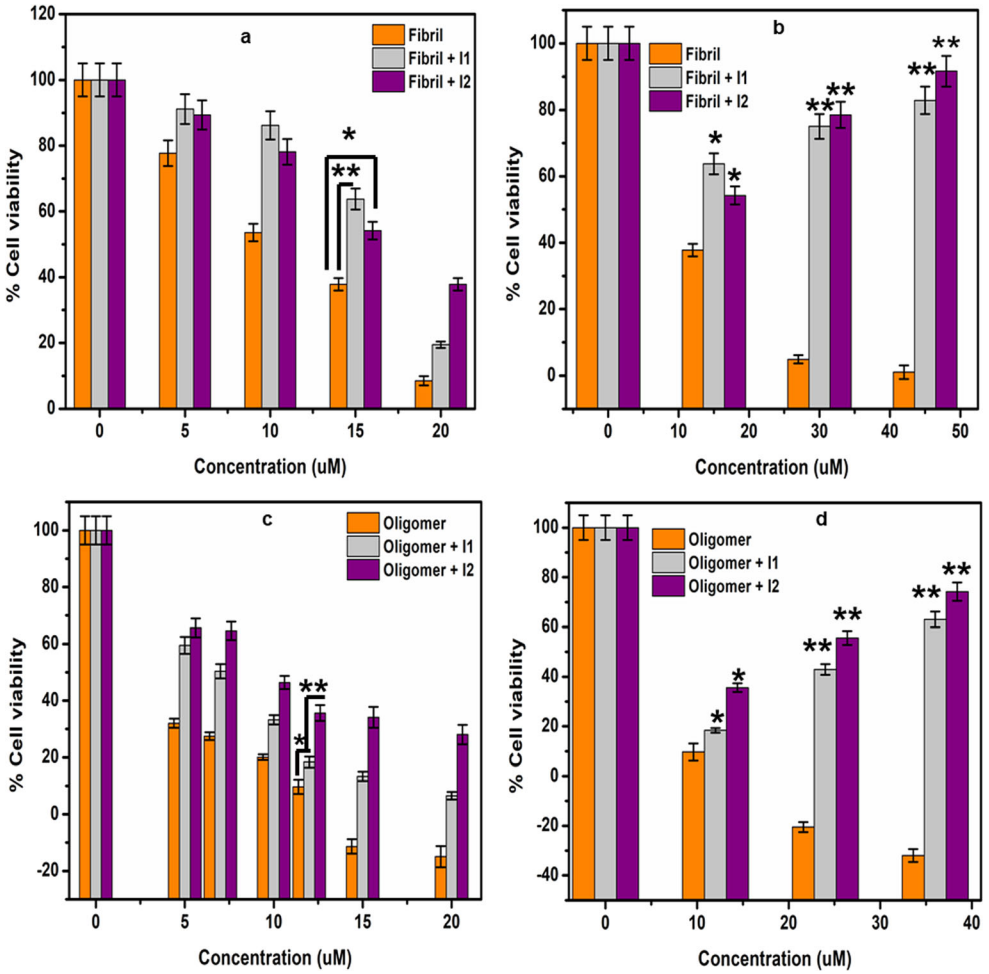

Fig. 6 Histogram showing % cell viability obtained in MTT assays. **a** Aβ_{42} fibrils and respective treatments with I1 & I2 in 1:1 molar ratio with the reference of control. The IC-50 value was found to be 15 μM of the fibril, and at this concentration I1 and I2 treated cells showed a significant recovery of cell viability with level of significance $*P < 0.05$ and $**P < 0.01$. **b** Increase in % cell viability for I1 and I2 treated cells in 1:1 to 1:3 molar ratios with respect to the control fibril and significance value $*P < 0.05$, $**P < 0.001$. **c** Aβ_{42} oligomers and respective treatments with I1 and I2 in 1:1 molar ratio with the reference of control. The IC-50 value was found to be 12 μM of oligomer concentration. Here, I1 and I2 treated cells showed a significant recovery of cell viability with $*P < 0.05$ and $**P < 0.01$ significance value. **d** Increase in % cell viability for I1 and I2 treated cells in 1:1 to 1:3 molar ratios with respect to the control oligomer and significance value $*P < 0.05$, $**P < 0.001$. The error bars indicate the standard error of mean from 3 experimental data

fact that the fibril was losing its structural integrity while interacting with the ligand [69].

In addition to structural signatures, weakening of the fibril was also evident from energy analysis (Fig. 8). A decrease in the interaction energy between the uppermost neighboring chains of fibril was accompanied by increased interaction between the exposed chain of the fibril and the ligand (Fig. S11). This analysis further suggested that due to the stable interaction between the ligand and the upper chain of the fibril, the interaction between neighboring chains of the fibril got weaker, and this eventually led to the fragmentation of the fibril [27, 70]. The complete fragmentation of fibril may occur in a time scale beyond the reach of these current computational studies. Nonetheless, the evidence of weakened interaction between the chains of fibril did indeed hint at the fragmentation of the fibril. The residue-wise decomposition of the interaction energy suggested that the LVF unit of the exposed chain (PROR) of Aβ_{42}-fibril contributes about 20% to the overall interaction energy between the ligand and the exposed chain (PROR) of the fibril (Fig. 8).

The signature of the initiation of fragmentation of the fibril in the presence of the ligand was also evident from the secondary structure analyses. The average number of amino acid residues participating in β-sheet conformation in the presence and absence of the ligand remained the same for those chains of the fibril that were not exposed to the ligand. However, the exposed and their neighboring chains projected a significant reduction in the number of β-sheet-forming amino acid residues in the presence of the ligand (Fig. S12a, b). This suggested that the fibril upon interaction with ligand underwent a change in its secondary structure which was very crucial in retaining the fibrillar structure.

Similar results were also obtained from the analysis of MD simulation of the ligand with oligomers (data not shown).

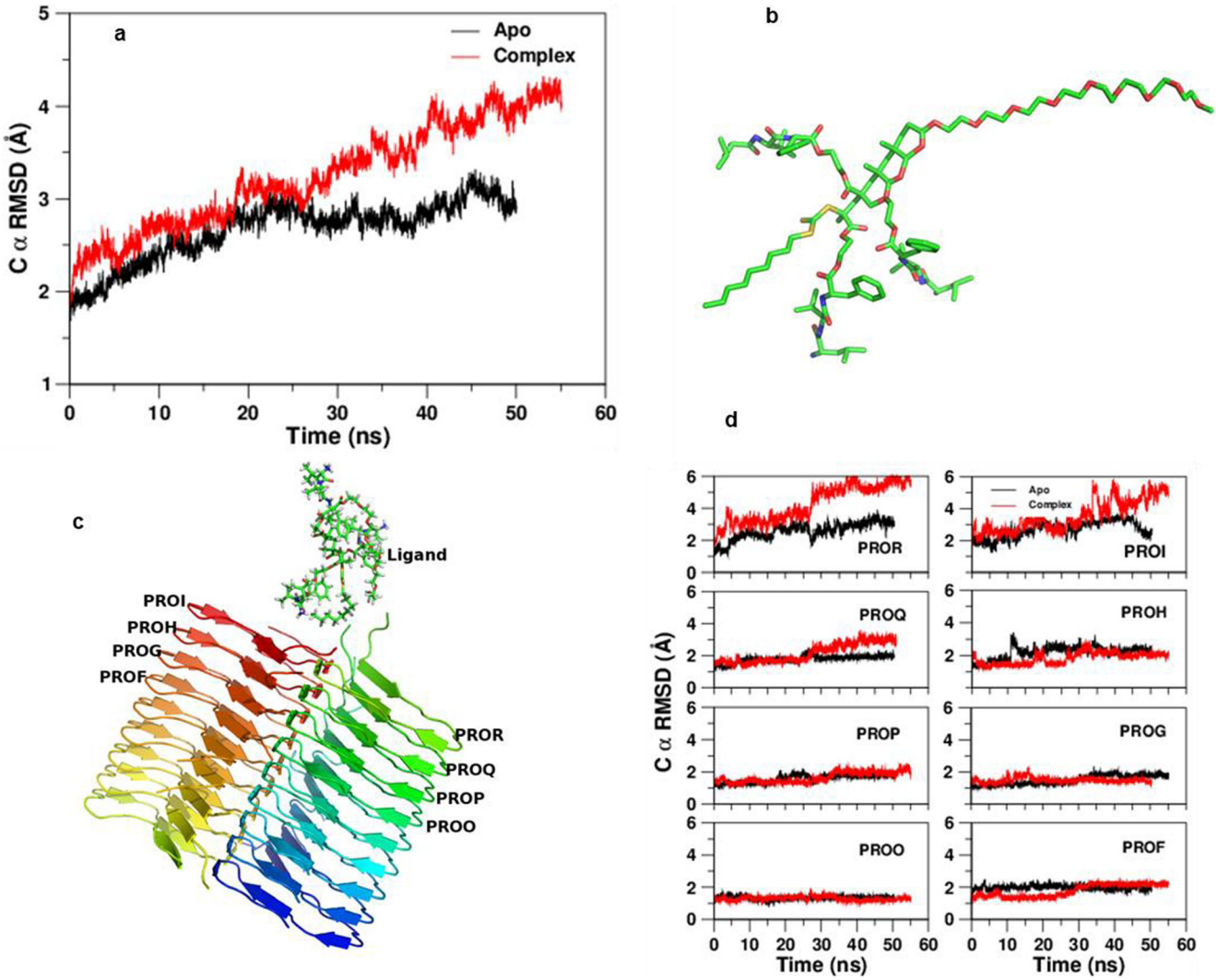

Fig. 7 **a** The root mean square deviation in Å of Cα atoms of apo (fibril) and complex (fibril with ligand). **b** A sticks representation of PEGylated inhibitor compound. **c** A cartoon representation of fibril with ligand shown as sticks. **d** The root mean square deviation in Å of Cα atoms of different monomeric units of fibril

Taken together, the present analysis established that the ligand not only interacts with monomer chains, thereby reducing the chance of aggregation, but also interacts with fibrils leading to their eventual fragmentation.

The binding kinetics of $A\beta_{42}$ monomers, as well as fibrils with the inhibitors, was validated with the aid of isothermal titration calorimetry (ITC) experiments in the support of the simulation studies. The calorimetric data, binding thermograms, and the associated thermodynamic parameters shown in Fig. S13 and Table S3 presented the binding affinity of I1 and I2 towards $A\beta_{42}$ monomeric population and $A\beta_{42}$ fibril as well. Most interestingly, it was found that the interaction of I1 and I2 with $A\beta_{42}$ monomers led to exothermic reaction with ΔH values −72,380 and -1.070×10^{9} Cal/mol, respectively. The change of entropy during these reactions suggested the stabilization of the $A\beta_{42}$ monomer due to binding with I1 and I2, respectively. In contrast, binding of the inhibitors with the $A\beta_{42}$ fibril was exhibited as an endothermic reaction. This signified that the energy absorbed during inhibitor–fibril interaction provided the energy to degrade the fibrils by I1 and I2.

Discussion

In spite of the emergence of a new drug candidate almost every day, there is still no clue for the treatment of the Alzheimer's disease. A previously reported side chain tripeptide-based PEGylated block copolymer has been shown to form a drug vehicle with its self-assembling property [40]. In some other previous literature, there was a hint on the possible potential inhibition of $A\beta_{42}$ fibril formation by the derivatives of short peptides containing hydrophobic stretch [29]. In the present study, a modified version of the side chain "leu-val-phe"-based PEGylated block copolymer has been tested for its β-sheet

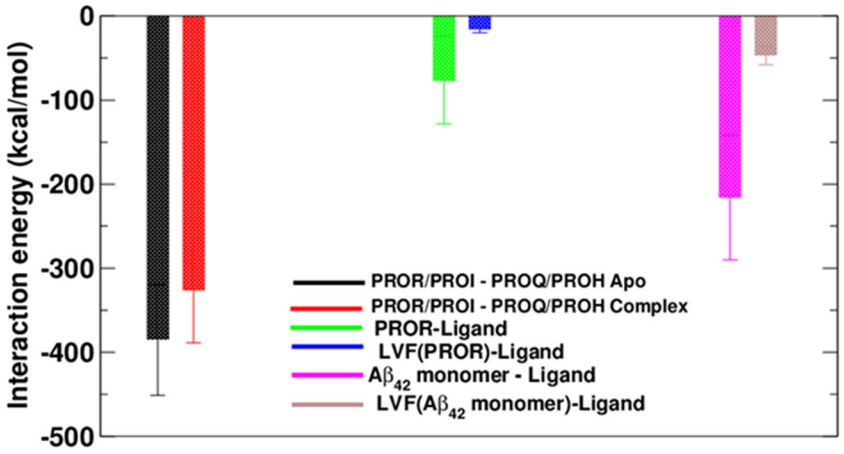

Fig. 8 The average interaction energy (electrostatic and van der Waals) between the two uppermost chains of Aβ_{42} fibril during 50 ns MD simulation of apo (fibril) and complex (fibril with ligand) (black and red, respectively). The average interaction energy between the ligand and the exposed monomer (PROR) unit in Aβ_{42} fibril (green) and the contribution of the LVF residues of PROR unit to this interaction energy (blue). The average interaction energy between the ligand and Aβ_{42} monomer (magenta) and the contribution of LVF residues of Aβ_{42} monomer (brown) to this interaction energy. In the exposed monomer of Aβ_{42} fibril as well as in the Aβ_{42} monomer, the LVF residues contribute about 20% to the overall interaction energy of the chain with the ligand

breaking properties. The assumption was to exploit the competitive binding of self-assembling "leu-val-phe" tripeptide of the block copolymer with a growing Aβ_{42} fibril chain. The PEGylated inhibitors performed well to demonstrate the competitive inhibition of a growing Aβ_{42} fibril when tested by the ThT assays. I2 exhibited an instant inhibition of oligomerization from the initial stage of Aβ_{42} fibril growth, whereas I1 was able to degrade the preformed fibrils after a certain time. In the DLS measurement, the presence of monomeric and/or oligomeric fractions of Aβ_{42} in the solution even after the 5th day of treatment ensures the binding of the inhibitor with its target Aβ_{42} and the retention of soluble monomers and/or oligomers in the solution which could not revert back into long fibrils again. The retention of the degraded fragments of fibrils as well as that of the oligomers even after 5 days of treatment was successfully demonstrated through the microscopic images also. With the aid of the biophysical techniques viz. CD and FTIR, the secondary structure of Aβ_{42} in the presence and absence of the inhibitors was evaluated. At its native state, Aβ_{42} peptide possesses a random coil or α-helical conformation [71, 72]. The conversion of Aβ peptide monomers into fibril results in switching of the α-helix or coiled structure into the β-sheet conformation [73, 74]. In our findings, the increase in delta ellipticity at 216 nm wavelength reflected this fact. Upon treatment with I1 and I2, the β-sheet rich conformation of fibril was completely destroyed and there was no peak showed at 208 nm and/or 222 nm which represents the characteristics of β-sheet rich conformation. The positive peak at 196 nm representing the β-sheet turns in the Aβ_{42} fibril was also diminished as shown in Fig. 5, in the case of I1 and I2-treated fibrils. In the support of the CD spectral change, the FTIR analyses also manifested the disappearance of the β-sheet-rich structure in treated Aβ_{42} fibrils. The switching from α-helix to β-sheet during fibrillization of Aβ_{42} and again destruction of characteristic β-sheet on undergoing treatment with both the inhibitors was evidenced from the changes in characteristic absorbance peaks. The decrease of the percent occurrence of β-sheet conformation from 52.37 to 19.38% and 19.73% in the case of I1- and I2-treated fibrils also complemented the fact of characteristic absorbance change. The non-toxic nature of the present block copolymers was proved by the cell survival assays. When we examined the improvement in cell viability upon treatment with the inhibitors with respect to the control fibril and oligomer, the data evinced the capability of the inhibitors to degrade the preformed fibril and oligomers. Thus, I1 and I2 helped the cells to cope up the toxic microenvironment. The results obtained so far led us to portrait the mechanism of action of the inhibitors. The assumption in this regard was to demolish the inter-chain hydrophobic interactions of the 16–22 amino acid residue-long hydrophobic core of the individual Aβ_{42} peptide. According to our hypothesis, the side chain tripeptide, i.e., "leu-val-phe," of the block copolymers should compete with the intra-chain hydrophobic interaction of the growing Aβ_{42} fibril and facilitate the competitive inhibition. According to Sun et al., Aβ16–22 forms multilayer cross-β aggregates through the self-assembly of single layer β-sheets [68]. Our investigation on the aggregation of "KLVFFA" segment of Aβ_{42} in the absence and presence of the inhibitor in molecular dynamics study revealed the interference of the inhibitors in the self-assembly of the segment during an 80 ns run. The increment in the RMSD fluctuation of C_α atoms of the exposed chain of the Aβ_{42} peptide on interacting with the inhibitor was an indication of fibril degradation. Moreover, upon interaction with the ligand, the exposed chain and also their neighboring chains of Aβ_{42} fibril exhibited a significant reduction in the β-sheet forming amino acid residues which was in complete agreement with the CD and FTIR data projecting the secondary structure deformation of a growing chain of the Aβ_{42} fibril. In addition, the black box simulations taking the "KLVFFA" segments of Aβ_{42} monomers

in the absence and presence of the inhibitor showed a general tendency of the monomeric units to come closer in the absence of the inhibitor and repulsion against their self-aggregation when the inhibitor was bound to a particular "KLVFFA" unit. The simulation studies theoretically projected an endothermic interaction between the Aβ_{42} fibril and ligand as shown in Fig. 8. This fact was practically proved via ITC experiments involving the degradation of the preformed fibrils of Aβ_{42} which manifested an endothermic reaction to take place. Interestingly, a closer look into the interaction energy contribution of the LVF tripeptide of the block copolymer for both the monomer-inhibitor and fibril-inhibitor interaction revealed about 20% involvement of LVF units. This confirms the possibility of competitive inhibition of side chain tripeptide as the mechanism of action of the inhibitors.

Conclusions

In conclusion, the PEGylated side chain tripeptidic block copolymers demonstrated challenging dynamicity of Aβ_{42} fibrillization pathway, targeting the very initial monomer to oligomer conversion, and, also, the aggregation of oligomers giving rise to the senile plaques. The results showing the inhibitory actions of the compounds pave the way towards extensive in vivo studies with the AD mice model which may envision a future clinical phase trial. The mechanism of drug action lies in being the competitive inhibitor of the hydrophobic stretch of Aβ_{42}. Our findings also reveal the shortest hydrophobic stretch (LVF) in the pathogenic Aβ_{42} peptide, responsible for playing the crucial role in peptide aggregation. In the future, the present block copolymers may be modified and constructed as nano drug carriers, impregnated with a symptomatic drug like Memantine or Acetylcholinesterase inhibitors, and can appear as new combinatorial therapeutic for AD.

Acknowledgements We thank Mr. Kashinath Sahu at the Indian Institute of Science Education and Research (IISER), Kolkata, and Mr. Satyabrata Samaddar at the CSIR—Indian Institute of Chemical Biology (IICB), Kolkata, for the assistance with the FE-SEM and FT-IR work, respectively.

Funding This research did not receive any specific grant from funding agencies in the public, commercial, or not-for-profit sectors.

Compliance with Ethical Standards

Conflicts of Interest The authors declare that they have no conflict of interest.

References

1. Khachaturian ZS (1985) Diagnosis of Alzheimer's disease. Arch Neurol 42:1097–1105
2. Oddo S, Caccamo A, Shepherd JD, Murphy MP, Golde TE, Kayed R, Metherate R, Mattson MP et al (2003) Triple-transgenic model of Alzheimer's disease with plaques and tangles: intracellular Aβ and synaptic dysfunction. Neuron 39:409–421
3. Reitz C, Brayne C, Mayeux R (2011) Epidemiology of Alzheimer disease. Nat Rev Neurol 7:137–152
4. Alzheimer's Association (2018) Alzheimer's disease facts and figures. Alzheimers Dement 14:367–429. https://doi.org/10.1016/j.jalz.2018.02.001
5. Khalsa DS, Perry G (2017) The four pillars of Alzheimer's prevention. Cerebrum: The Dana Forum on Brain Science. 2017:cer-03-17. https://www.ncbi.nlm.nih.gov/pmc/articles/PMC5501038/. Accessed 1 Mar 2017
6. Prince M, Comas-Herrera A, Knapp M, Guerchet M, Karagiannidou M (2016) World Alzheimer report 2016: The global impact of dementia. Alzheimer's Disease International (ADI), London
7. Hardy JA, Higgins GA (1992) Alzheimer's disease: the amyloid cascade hypothesis. Science 256:184–185
8. Maccioni RB, Farías G, Morales I, Navarrete L (2010) The revitalized tau hypothesis on Alzheimer's disease. Arch Med Res 41:226–231
9. Swerdlow RH, Burns JM, Khan SM (2014) The Alzheimer's disease mitochondrial cascade hypothesis: progress and perspectives. Biochim Biophys Acta 1842:1219–1231
10. Chételat G, Villemagne VL, Bourgeat P (2010) Relationship between atrophy and β-amyloid deposition in Alzheimer disease. Ann Neurol 67:317–324
11. Greenough MA, Camakaris J, Bush AI (2013) Metal dyshomeostasis and oxidative stress in Alzheimer's disease. Neurochem Int 62:540–555
12. Hane F (2013) Are amyloid fibrils molecular spandrels? FEBS Lett 587:3617–3619
13. Benilova I, Karran E, De Strooper B (2012) The toxic Aβ oligomer and Alzheimer's disease: an emperor in need of clothes. Nat Neurosci 15:349–357
14. Dutta S, Foley AR, Warner CJ (2017) Suppression of oligomer formation and formation of non-toxic fibrils upon addition of mirror-image Aβ42 to the natural l-enantiomer. Angew Chem Int Ed 56:11506–11510
15. Haass C, Selkoe DJ (2007) Soluble protein oligomers in neurodegeneration: lessons from the Alzheimer's amyloid β-peptide. Nat Rev Mol Cell Biol 8:101–112
16. Hardy J, Selkoe DJ (2002) The amyloid hypothesis of Alzheimer's disease: progress and problems on the road to therapeutics. Science 297:353–356
17. Sullivan MG (2017) Alzheimer's candidate drug Aducanumab moves to phase III. Caring for the Ages 18:18. https://doi.org/10.1016/j.carage.2017.02.015
18. Gao N, Sun H, Dong K, Ren J, Qu X (2015) Gold-nanoparticle-based multifunctional amyloid-β inhibitor against Alzheimer's disease. Chem Eur J 21:829–835
19. Geng J, Li M, Ren J, Wang E, Qu X (2011) Polyoxometalates as inhibitors of the aggregation of amyloid β peptides associated with Alzheimer's disease. Angew Chem Int Ed 123:4270–4274
20. Li M, Xu C, Ren J, Wang E, Qu X (2013) Photodegradation of β-sheet amyloid fibrils associated with Alzheimer's disease by using polyoxometalates as photocatalysts. Chem Commun 49:11394–11396
21. Wong HE, Qi W, Choi HM, Fernandez EJ, Kwon I (2011) A safe, blood-brain barrier permeable triphenylmethane dye inhibits amyloid-β neurotoxicity by generating nontoxic aggregates. ACS Chem Neurosci 2:645–657
22. Cohen SI, Arosio P, Presto J et al (2015) A molecular chaperone breaks the catalytic cycle that generates toxic Aβ oligomers. Nat Struct Mol Biol 22:207–213

23. Evans CG, Wisén S, Gestwicki JE (2006) Heat shock proteins 70 and 90 inhibit early stages of amyloid β-(1–42) aggregation in vitro. J Biol Chem 281:33182–33191
24. McKoy AF, Chen J, Schupbach T, Hecht MH (2012) A novel inhibitor of amyloid β (Aβ) peptide aggregation from high throughput screening to efficacy in an animal model of Alzheimer disease. J Biol Chem 287:38992–39000
25. Rezai-Zadeh K, Shytle D, Sun N, Mori T, Hou H, Jeanniton D, Ehrhart J, Townsend K et al (2005) Green tea epigallocatechin-3-gallate (EGCG) modulates amyloid precursor protein cleavage and reduces cerebral amyloidosis in Alzheimer transgenic mice. J Neurosci 25:8807–8814
26. Soto C, Sigurdsson EM, Morelli L, Kumar RA, Castaño EM, Frangione B (1998) β-Sheet breaker peptides inhibit fibrillogenesis in a rat brain model of amyloidosis: implications for Alzheimer's therapy. Nat Med 4:822–826
27. Han X, Park J, Wu W, Malagon A, Wang L, Vargas E, Wikramanayake A, Houk KN et al (2017) A resorcinarene for inhibition of Aβ fibrillation. Chem Sci 8:2003–2009
28. Mukhopadhyay CD, Ruidas B, Chaudhury SS (2017) Role of curcumin in treatment of Alzheimer disease. Int J Neurorehabilitation 4:274
29. Skaat H, Chen R, Grinberg I, Margel S (2012) Engineered polymer nanoparticles containing hydrophobic dipeptide for inhibition of amyloid-β fibrillation. Biomacromolecules 13:2662–2670
30. Bachurin SO, Bovina EV, Ustyugov AA (2017) Drugs in clinical trials for Alzheimer's disease: the major trends. Med Res Rev 37: 1186–1225
31. Cummings JL, Morstorf T, Zhong K (2014) Alzheimer's disease drug-development pipeline: few candidates, frequent failures. Alzheimers Res Ther 6:37
32. Mangialasche F, Solomon A, Winblad B, Mecocci P, Kivipelto M (2010) Alzheimer's disease: clinical trials and drug development. Lancet Neurol 9:702–716
33. Schneider LS, Mangialasche F, Andreasen N, Feldman H, Giacobini E, Jones R, Mantua V, Mecocci P et al (2014) Clinical trials and late-stage drug development for Alzheimer's disease: an appraisal from 1984 to 2014. J Intern Med 275:251–283
34. Cheng YS, Chen ZT, Liao TY, Lin C et al (2017) An intranasally delivered peptide drug ameliorates cognitive decline in Alzheimer transgenic mice. EMBO Mol Med 9:703–715
35. Taylor M, Moore S, Mayes J, Parkin E, Beeg M, Canovi M, Gobbi M, Mann DMA et al (2010) Development of a proteolytically stable retro-inverso peptide inhibitor of β-amyloid oligomerization as a potential novel treatment for Alzheimer's disease. Biochemistry 49: 3261–3272
36. Som Chaudhury S, Das Mukhopadhyay C (2018) Functional amyloids: interrelationship with other amyloids and therapeutic assessment to treat neurodegenerative diseases. International Journal of Neuroscience 128:449–463
37. De Santis S, Chiaraluce R, Consalvi V et al (2017) PEGylated β-sheet breaker peptides as inhibitors of β-amyloid fibrillization. Chempluschem 82:241–250
38. Zhang C, Zheng X, Wan X, Shao X, Liu Q, Zhang Z, Zhang Q (2014) The potential use of H102 peptide-loaded dual-functional nanoparticles in the treatment of Alzheimer's disease. J Control Release 192:317–324
39. Zheng X, Shao X, Zhang C, Tan Y, Liu Q, Wan X, Zhang Q, Xu S et al (2015) Intranasal H102 peptide-loaded liposomes for brain delivery to treat Alzheimer's disease. Pharm Res 32:3837–3849
40. Kumar S, Acharya R, Chatterji U, De P (2014) Controlled synthesis of β-sheet polymers based on side-chain amyloidogenic short peptide segments via RAFT polymerization. Polym Chem 5:6039–6050
41. Reinke AA, Gestwicki JE (2007) Structure–activity relationships of amyloid beta-aggregation inhibitors based on curcumin: influence of linker length and flexibility. Chem Biol Drug Des 70:206–215
42. Saleem S, Biswas SC (2017) Tribbles pseudokinase 3 induces both apoptosis and autophagy in amyloid-β-induced neuronal death. J Biol Chem 292:2571–2585
43. Lee KH, Shin BH, Shin KJ, Kim DJ, Yu J (2005) A hybrid molecule that prohibits amyloid fibrils and alleviates neuronal toxicity induced by β-amyloid (1–42). Biochem Biophys Res Commun 328:816–823
44. Ahmed M, Davis J, Aucoin D, Sato T, Ahuja S, Aimoto S, Elliott JI, van Nostrand WE et al (2010) Structural conversion of neurotoxic amyloid-β 1–42 oligomers to fibrils. Nat Struct Mol Biol 17:561–567
45. Dehle FC, Ecroyd H, Musgrave IF, Carver JA (2010) αB-Crystallin inhibits the cell toxicity associated with amyloid fibril formation by κ-casein and the amyloid-β peptide. Cell Stress Chaperones 15: 1013–1026
46. Colvin MT, Silvers R, Ni QZ, Can TV, Sergeyev I, Rosay M, Donovan KJ, Michael B et al (2016) Atomic resolution structure of monomorphic Aβ42 amyloid fibrils. J Am Chem Soc 138:9663–9674
47. Pham JD, Spencer RK, Chen KH, Nowick JS (2014) A fibril-like assembly of oligomers of a peptide derived from β-amyloid. J Am Chem Soc 136:12682–12690
48. Crescenzi O, Tomaselli S, Guerrini R, Salvadori S, D'Ursi AM, Temussi PA, Picone D (2002) Solution structure of the Alzheimer amyloid β-peptide (1–42) in an apolar microenvironment: similarity with a virus fusion domain. Eur J Biochem 269:5642–5648
49. Colletier JP, Laganowsky A, Landau M, Zhao M, Soriaga AB, Goldschmidt L, Flot D, Cascio D et al (2011) Molecular basis for amyloid-β polymorphism. Proc Natl Acad Sci U S A 108:16938–16943
50. Phillips JC, Braun R, Wang W, Gumbart J, Tajkhorshid E, Villa E, Chipot C, Skeel RD et al (2005) Scalable molecular dynamics with NAMD. J Comput Chem 26:1781–1802
51. MacKerell AD Jr, Bashford D, Bellott ML et al (1998) All-atom empirical potential for molecular modeling and dynamics studies of proteins. J Phys Chem B 102:3586–3616
52. Jorgensen WL, Madura JD (1983) Solvation and conformation of methanol in water. J Am Chem Soc 105:1407–1413
53. Vanommeslaeghe K, Hatcher E, Acharya C, Kundu S, Zhong S, Shim J, Darian E, Guvench O et al (2010) CHARMM general force field: a force field for drug-like molecules compatible with the CHARMM all-atom additive biological force fields. J Comput Chem 31:671–690
54. Humphrey W, Dalke A, Schulten K (1996) VMD: visual molecular dynamics. J Mol Graph 14:33–38
55. DeLano WL (2009) The PyMOL molecular graphics system 2009. DeLano Scientific, San Carlos
56. Sannigrahi A, Maity P, Karmakar S, Chattopadhyay K (2017) Interaction of KMP-11 with phospholipid membranes and its implications in leishmaniasis: effects of single tryptophan mutations and cholesterol. J Phys Chem B 121:1824–1834
57. Jameson LP, Smith NW, Dzyuba SV (2012) Dye-binding assays for evaluation of the effects of small molecule inhibitors on amyloid (Aβ) self-assembly. ACS Chem Neurosci 3:807–819
58. Knight JD, Miranker AD (2004) Phospholipid catalysis of diabetic amyloid assembly. J Mol Biol 341:1175–1187
59. Li J, Tian C, Yuan Y, Yang Z, Yin C, Jiang R, Song W, Li X et al (2015) A water-soluble conjugated polymer with pendant disulfide linkages to PEG chains: a highly efficient ratiometric probe with solubility-induced fluorescence conversion for thiol detection. Macromolecules 48:1017–1025

60. Adochitei A, Drochioiu G (2011) Rapid characterization of peptide secondary structure by FT-IR spectroscopy. Rev Roum Chim 56: 783–791
61. Zandomeneghi G, Krebs MR, McCammon MG, Fändrich M (2004) FTIR reveals structural differences between native β-sheet proteins and amyloid fibrils. Protein Sci 13:3314–3321
62. Castelletto V, Ryumin P, Cramer R, Hamley IW, Taylor M, Allsop D, Reza M, Ruokolainen J et al (2017) Self-assembly and anti-amyloid cytotoxicity activity of amyloid beta peptide derivatives. Sci Rep 7:43637
63. Hubin E, Deroo S, Schierle GK, Kaminski C, Serpell L, Subramaniam V, van Nuland N, Broersen K et al (2015) Two distinct β-sheet structures in Italian-mutant amyloid-beta fibrils: a potential link to different clinical phenotypes. Cell Mol Life Sci 72: 4899–4913
64. Sarkar-Banerjee S, Chowdhury S, Paul SS, Dutta D, Ghosh A, Chattopadhyay K (2016) The non-native helical intermediate state may accumulate at low pH in the folding and aggregation landscape of the intestinal fatty acid binding protein. Biochemistry 55:4457–4468
65. Amini Z, Fatemi MH, Rauk A (2016) Molecular dynamics studies of a β-sheet blocking peptide with the full-length amyloid beta peptide of Alzheimer's disease. Can J Chem 94:833–841
66. Xu Y, Shen J, Luo X, Zhu W, Chen K, Ma J, Jiang H (2005) Conformational transition of amyloid β-peptide. Proc Natl Acad Sci U S A 102:5403–5407
67. Xie L, Luo Y, Wei G (2013) Aβ (16–22) peptides can assemble into ordered β-barrels and bilayer β-sheets, while substitution of phenylalanine 19 by tryptophan increases the population of disordered aggregates. J Phys Chem B 117:10149–10160
68. Zhang M, Chen J, Tian Z, Wang H (2017) Reply to the 'Comment on "Magnetic-field-enabled resolution enhancement in super-resolution imaging"' by Bergmann et al., Physical Chemistry Chemical Physics, 2017, 19. Phys Chem Chem Phys 19:4891–4892
69. Berhanu WM, Hansmann UH (2013) The stability of cylindrin β-barrel amyloid oligomer models—a molecular dynamics study. Proteins 81:1542–1555
70. Han X, Tian C, Gandra I, Eslava V, Galindres D, Vargas E, Leblanc R (2017) The investigation on Resorcinarenes towards either inhibiting or promoting insulin fibrillation. Chem Eur J 23: 17903–17907
71. Simmons LK, May PC, Tomaselli KJ, Rydel RE, Fuson KS, Brigham EF, Wright S, Lieberburg I et al (1994) Secondary structure of amyloid beta peptide correlates with neurotoxic activity in vitro. Mol Pharmacol 45:373–379
72. Soto C, Castaño EM, Kumar RA, Beavis RC, Frangione B (1995) Fibrillogenesis of synthetic amyloid-β peptides is dependent on their initial secondary structure. Neurosci Lett 200:105–108
73. Jarvet J, Damberg P, Bodell K, Göran Eriksson LE, Gräslund A (2000) Reversible random coil to β-sheet transition and the early stage of aggregation of the Aβ (12–28) fragment from the Alzheimer peptide. J Am Chem Soc 122:4261–4268
74. Sureshbabu N, Kirubagaran R, Jayakumar R (2009) Surfactant-induced conformational transition of amyloid β-peptide. Eur Biophys J 38:355–367